

Absence of molecular mobility on nano-second time scales in amorphous ice phases

M.M. Koza¹, B. Geil², H. Schober¹, F. Natali¹.

¹*Institut Laue-Langevin,*

F-38042 Grenoble Cedex, France.

²*Fachbereich Physik, TU Darmstadt,*

D-64289 Darmstadt, Germany.

(Dated: July 2, 2018)

Abstract

High-resolution neutron backscattering techniques are exploited to study the elastic and quasi-elastic response of the high-density amorphous (HDA), the low-density amorphous (LDA) and the crystalline ice I_c upon temperature changes. Within the temperature ranges of their structural stability (HDA at $T \leq 80$ K, LDA at $T \leq 135$ K, ice I_c at $T < 200$ K) the Debye-Waller factors and mean-square displacements characterise all states as harmonic solids. During the transformations HDA \rightarrow LDA ($T \approx 100$ K), LDA \rightarrow I_c ($T \approx 150$ K) and the supposed glass transition with $T_g \approx 135$ K no relaxation processes can be detected on a time scale $t < 4$ ns. It can be concluded from coherent scattering measurements (D₂O) that LDA starts to recrystallise into ice I_c at $T \approx 135$ K, i.e. at the supposed T_g . In the framework of the Debye model of harmonic solids HDA reveals the highest Debye temperature among the studied ice phases, which is in full agreement with the lowest Debye level in the generalised density of states derived from time-of-flight neutron scattering experiments. The elastic results at low T indicate the presence of an excess of modes in HDA, which do not obey the Bose statistics.

PACS numbers: 63.50.+x, 64.70.Kb, 78.70.Ck

I. INTRODUCTION

Water, although comprising one of the most simple molecules, reveals extremely complicated properties in its condensed states. In the solid state for example, there exist not only twelve well known crystalline phases but also a number of disordered structures [1, 2]. Two of the disordered structures are known as high-density amorphous (HDA) and low-density amorphous (LDA) ice, characterised by a molecular density of $\rho \approx 39$ molec./nm³ and $\rho \approx 31$ molec./nm³, respectively [3, 4]. The origin of a number of different disordered phases within a single substance, often referred to as amorphous polymorphism, has not been understood, yet. It has been conjectured on the basis of computer simulation results that HDA and LDA might represent the supercooled glassy structures of two different liquid phases of water [5, 6, 7, 8, 9]. Obviously, this scenario implies the existence of a glass-transition designated by a glass-transition temperature T_g .

From the experimental point of view, there is a number of results backing the findings from computer simulations. Structures equivalent to HDA and LDA can be obtained from the liquid by extremely fast quenching of μ m-droplets or from the gas phase by vapour deposition [10, 11, 12, 13, 14]. As far as LDA-type structures are concerned, they all transform exothermally to a crystalline cubic phase (ice I_c) at $T \approx 150 - 160$ K on an endothermal plateau setting in at $T \approx 135$ K, which has been observed by differential scan calorimetry (DSC) and other calorimetric experiments [16, 17, 18, 19, 20, 21, 22, 23, 24, 25, 26]. The very onset of the endothermal contribution has been interpreted as water's T_g in literature, whereby in LDA the lowest $T_g \approx 124$ K of all low-density amorphous structures is discussed [18].

A comparable T_g has been deduced from DSC studies of different aqueous solutions, whose specific T_g s extrapolate upon dilution toward the single value of 135 K [27, 28]. Finally, from observation of D₂O–H₂O interlayer mixing upon heating of LDA-type vapour deposited water a higher molecular mobility at $T \approx 150$ K has been concluded [29, 30].

However, these experimental results do not establish unequivocally a glass-transition or a glass-transition temperature in water. For each of the cited experiments there can be found at least one experiment *reported in literature* whose results either contrast the glass transition scenario or give an alternative explanation for the observed phenomena. For example, endothermal transitions have been observed at the same thermodynamic conditions

in transformations of high-density crystalline ice phases to ice I_c. They are understood as entropy driven order → disorder transitions in the proton sublattice of the phases [25, 31, 32] a feature equally detected in ice I_c [33]. In this context, it is noteworthy that recently well established DSC results on apparent LDA samples [19, 21, 23, 24] had to be reinterpreted as such a reversible order → disorder transition in the proton sublattice of ice XII [25]. The very low $T_g \approx 124$ K reported in [18] remains to be reexamined [25]. Consequently, one may ask what is the unique dynamic feature by which, on the one hand, the endothermic plateau in the amorphous systems is interpreted as a glass–transition but, on the other hand, it is identified in the crystalline structures as a disorder phenomenon of the proton sublattice only. Whether the recently observed endothermic effect in pressure dependent experiments on emulsified amorphous samples is a unique feature of the disordered system *requires equally a closer examination* [26].

In contrast to the D₂O–H₂O interlayer mixing effect [29, 30] ion diffusion experiments have not shown any higher mobility of guest molecules in the amorphous ice matrix [34] neither have isotopic exchange measurements shown any translational motion of water molecules [35]. Instead, they have given the picture of a defect promoted proton mobility responsible for the endothermic transition, a feature directly detectable by Nuclear Magnetic Resonance in crystalline ice and clathrate hydrates [36, 37].

Recently, models of a so called shadow glass–transition have been proposed that explain the thermal anomalies observed at $T \approx 135$ K with a real but experimentally unaccessible glass–transition at $T_g \approx 165$ K [38]. Whether this shadow glass–transition could be indeed applicable to water is the issue of current debates [39, 40].

Another idiosyncratic feature which has not been satisfactorily explained, yet, is the inelastic response of the amorphous ice structures. Dynamic properties of bulk HDA, LDA and LDA–type structures differ strongly from established features of supercooled glassy systems [41, 42]. The dynamic response of LDA does not exhibit any phonon damping [43, 44], any remarkable Boson–peak [44, 45, 46, 47], and any two–level systems (TLS) [48, 49, 50]. Consequently, its spectral density and thermal conductivity are reminiscent of a harmonic crystalline state [51]. In the case of HDA, this departure from the characteristics of glassy states is apparently less pronounced, since TLS modes have been unequivocally observed in optical absorption experiments [48, 49, 50]. Similar features are observed by inelastic neutron experiments [52, 53, 54], where an excess of modes in the density of vibrational

states is reported. However, the detailed phonon dispersion and also the spectral density at $T > 40$ K of HDA are identified as crystal-like in other experiments pointing at an intriguing high degree of short-range order [43, 55].

In the light of the above outlined experimental facts the idea of HDA and LDA being strongly disordered crystalline systems not thermodynamically connected to water's liquid phase [56], may at first glance seem rather tempting. Such a nano-crystalline scenario has been discussed for water [56] but also for other systems showing amorphous polymorphism [57]. A discontinuity between the liquid state, vapour deposited and hyper-quenched amorphous water on the one hand and LDA on the other hand has been indeed postulated based on theoretical concepts and results from spectroscopic experiments and computer simulations [58, 59, 60, 61]. Giving the subject some further thinking it becomes, however, obvious that a nano-crystalline scenario does not provide a more stringent explanation for the absence of glassy features in the dynamics. The inherently high disorder within the nano-crystals should leave a clear trace in the low-frequency dynamics not too different from that of a glassy state.

To advance the question further it is obviously indispensable to characterize the fundamental, microscopic relaxation processes responsible for the endothermic plateau in DSC experiments. This characterization must be carried out both in time and space. While order-disorder phenomena and the glass relaxation may take place on similar time scales the spatial correlations are different. In particular, the spatial patterns should allow to discern the hypothetical relaxation channels of the glass-transition from processes observed during the transitions of high-density crystalline structures to ice I_c .

The present work represents our first attempt of scrutinizing the glass-transition hypothesis of water with a supposed $T_g \approx 135$ K on a microscopic scale by neutron backscattering and time-of-flight techniques, i.e. by spectroscopic techniques sampling time and spatial correlations. Both techniques have been extensively used for studying glass transition phenomena and proved to be substantial for their understanding. Both, time-of-flight and backscattering spectroscopy offer the opportunity of studying the microscopic dynamics of a sample directly as an energy resolved response. In addition, neutron backscattering can be also used to exploit the elastic scattering within a narrow energy range $\sim 1 \mu\text{eV}$ from which important dynamic properties can be deduced [62, 63]. This enables us, in principle, to characterise relaxation processes on a molecular scale during the apparent glass-transition.

All experiments performed reveal that the properties of HDA and LDA follow a temperature dependence in complete accordance with the harmonic theory of the solid state [63, 64]. Beyond the low-temperature limit, where zero-point oscillations are predominant, the molecular mean-square displacements of HDA and LDA are proportional to the temperature increase. This behaviour is expected if the degrees of freedom, and thus the spectral density of the sample in its different states is determined by harmonic modes only. The very good conformity with the mean-square displacements deduced from the phonon densities of states of HDA and LDA reinforces this scenario. In the temperature regime of the transitions HDA \rightarrow LDA and LDA \rightarrow ice I_c comprising the apparent glass-transition with $T_g \approx 135$ K no higher mobility of water molecules, e.g., in terms of translational diffusion, is observed on a time scale shorter than some nano-seconds. From experiments on coherently scattering samples the temperature $T \approx 135$ K is identified as the onset of a recrystallisation of LDA into ice I_c [65]. In addition, an excess of modes in HDA, that however does not follow the Bose-statistics valid for harmonic vibrations, is clearly indicated in the values of the zero-point oscillation.

To bring these findings clearly forward the present paper is structured in the following way. The next two chapters render some useful details on the applied neutron scattering techniques, the samples and experimental procedure, and introduce some observables (Debye-Waller factor, mean-square displacement, density of states, velocity of sound), to which we refer throughout the text. In section IV, we present and discuss the experimental data in view of the studied transitions (HDA \rightarrow LDA, LDA \rightarrow I_c, and the glass-transition), the Debye-Waller factor and mean-square displacement, and the excess of modes in HDA. All results obtained are summarised in section V.

II. EXPERIMENTAL

To meet the requirement of high energy resolution the experiments have been performed on the neutron backscattering spectrometers IN13 and IN16 and the time-of-flight spectrometer IN6 at the Institut Laue Langevin in Grenoble, France [66]. The principles of the backscattering spectrometers are based on the neutron beam monochromatization and the

energy analysis of the scattered beam by single crystal Bragg reflection

$$n \cdot \lambda = 2d \sin(\Theta) \quad (1)$$

in backscattering geometry $\Theta \approx 90^\circ$ [62, 63]. Using the $\text{CaF}_2(422)$ reflection on IN13 and the $\text{Si}(111)$ on IN16 the incident neutron energies (E) and energy resolutions (ΔE) of $E = 16.5 \text{ meV}$, $\Delta E = 8 \mu\text{eV}$ and $E = 2 \text{ meV}$, $\Delta E = 1 \mu\text{eV}$ are obtained, respectively. Beyond the differences in incident energy and energy resolution these spectrometers are optimised for sampling complementary Q -ranges. IN16 with $Q < 2.1 \text{ \AA}^{-1}$ is best utilised for e.g. long range diffusion processes with a correlation length of $r > 3 \text{ \AA}$. IN13 with $Q < 5.5 \text{ \AA}^{-1}$ is optimised for short range diffusion with $r > 1 \text{ \AA}$. Thus, with both instruments we are able to cover a spatial range stretching from correlations within the proton sublattice of water up to its intermolecular distances.

In general, backscattering spectrometers can be utilised in two different modes. Firstly, in the elastic scan mode, the incident neutron energy is kept constant to permanently meet the Bragg condition of the analyser given by eq. 1. The elastic scan mode samples changes of the elastic intensity within ΔE due to dynamic and relaxation processes which may be induced by changing experimental parameters like temperature in the present case. Secondly, in the energy scan mode, the incident neutron energy is varied in a well defined, systematic way within a narrow energy range δE , e.g., $\delta E \approx \pm 10 \mu\text{eV}$ on IN16. In the energy scan mode, dynamic and relaxation processes can be, in principle, characterised quantitatively. Both, energy and elastic scan mode, were applied on the spectrometer IN16 whereas IN13 was used in the elastic scan mode exclusively.

The time-of-flight spectrometer IN6 was used with incident energies of 3.1 meV ($\Delta E = 80 \mu\text{eV}$) and 4.8 meV ($\Delta E = 150 \mu\text{eV}$). The sampled Q -ranges of $0.3\text{--}2.1 \text{ \AA}^{-1}$ (3.1 meV) and $0.3\text{--}2.6 \text{ \AA}^{-1}$ (4.8 meV) matched the Q regime of the IN16 measurements. However, the energies probed by the instrument IN6 correspond to dynamic processes on a time scale of $\tau < 50 \text{ pico--seconds}$.

In detail, we studied two fully protonated samples on IN16, one sample, S3, in elastic scan and a second, S4, in energy scan mode, and two samples on IN13, sample S2 fully deuterated and sample S1 partially protonated with 40% vol. H_2O . Three fully deuterated samples were measured on IN6. The deuteration was employed for a better control of the sample state via the pronounced coherent scattering contribution of D_2O to the signal and

for an enhanced signal contribution from the Oxygen atoms. Figure 1 shows the elastic intensity $I(Q, \omega = 0)$ of the samples S1 and S2 in the HDA and the LDA state in comparison to the structure factor $S(Q) = \int S(Q, \omega) d\omega$ of fully deuterated HDA and LDA measured with high resolution on the diffractometer D20 at the Institut Laue Langevin [67]. The coherent signal of the partially protonated sample is, as expected, strongly suppressed and the scattering characteristics are reminiscent of the incoherent contribution.

All samples were prepared by compression of crystalline ice I_h at $T \approx 77$ K (in liquid N₂) in a piston–cylinder apparatus up to $p \approx 18$ kbar [68]. The formed HDA was recovered at ambient pressure, filled into Aluminum holders used as standard in neutron scattering and placed into precooled ($T = 75$ K) standard cryostats. After remaining N₂ had been carefully removed at $T = 78$ K the samples were cooled down to $T = 2$ K. Table I gives details on the thermal treatment and thermal cycling applied to the samples during the experiments. Data were accumulated on IN13 for 60 min per point with the samples gradually heated corresponding with a rate of 3.5 K/60 min. IN16 elastic scan data were accumulated for 2 min with a heating rate of 1 K/2 min. IN16 inelastic scan data were accumulated for 2×90 min with a heating step of 2 K in the range of the supposed glass transition, whereby *in situ* data updates were performed every 10 min giving, within the data statistics, identical results as obtained after 90 min acquisition time. As for the LDA state the thermal treatments resulted in phases which had been annealed for 2 h at 125 K plus 1 h at 128.5 K on IN13 and for 1 h at 130 K and a preceding slow heating on IN16 before the regime of the apparent glass transition was reached. Thus, annealing times and heating rates corresponded with treatments performed in DSC experiments on water's T_g reported in literature.

Samples measured at IN6 were subject to a comparable thermal cycling procedure whereby the LDA structure was annealed at 127 K and ice I_c was annealed at 160 K. Measurements following the glass–transition have been performed at the temperatures $T = 127$ K for 4×60 min., at $T = 132$ K for 4×60 min., at $T = 137$ K for 5×30 min., at $T = 140$ K for 6×30 min., at $T = 143$ K for 4×30 min., at $T = 147$ K for 30 min. and at $T = 155$ K for 30 min. before annealing the formed ice I_c at 160 K. Long time measurements of 4–6 hours were carried out with HDA at 2 K, 20 K, 40 K, 60 K and 80 K, with LDA at 2 K, 20 K, 40 K, 60 K, 80 K and 127 K, and ice I_c at 127 K and 160 K.

Standard data corrections were performed, accounting for empty container and background scattering, self-shielding, absorption effects of the samples and for efficiencies of

TABLE I: Thermal cycling applied to the samples S1 and S2 (IN13) and S3 and S4 (IN16). The phases given below indicate the states in which the samples existed when heat treatment was started at 2 K for the measurements. Please note that S1 was measured twice within the stability range of HDA.

phase	sample S1	sample S2	sample S3	sample S4
HDA	2→65→2→125 K	2→125 K	2→130 K	2→160 K
LDA	2→170 K	2→170 K	2→260 K	–
ice I _c	2→170 K	–	–	–

the instrument detectors. However, due to the scattering power of the samples (optimised for multiple scattering behaviour) and the negligible absorption of the scatterers only minor perturbations of the signal were observed. Nevertheless, the elastic signal measured in the low- Q range on the spectrometer IN16 encounters a lower sensitivity to temperature changes in comparison to the results taken on IN13. This feature is well reported in literature and associated with contribution from multiple scattering processes [69]. Depending on the information which is to be extracted from the experimental data, different normalisation standards have to be used. These standards are explicitly described in the text below.

For a clear presentation of the extensive amount of data some data sets have been regrouped to give statistical errors of the order of the data symbols. Error bars are plotted with the data in the figures. The grouping is explicitly indicated in the figure captions for data whose interpretation exceeds a pure qualitative description. All fitting routines were performed with ungrouped data sets. The simplex minimization algorithm was applied having taken into account the x-grid and y-error of the fitted data.

Please note, that we focus primarily on the backscattering measurements due to the superior resolution of the instruments, when discussing potential relaxation processes during the phase transitions HDA to LDA and LDA to ice I_c.

III. OBSERVABLES IN NEUTRON SCATTERING

For the convenience of the reader let us summarise some basic principles of neutron scattering as they are needed for the comprehension of the data analysis and the discussion.

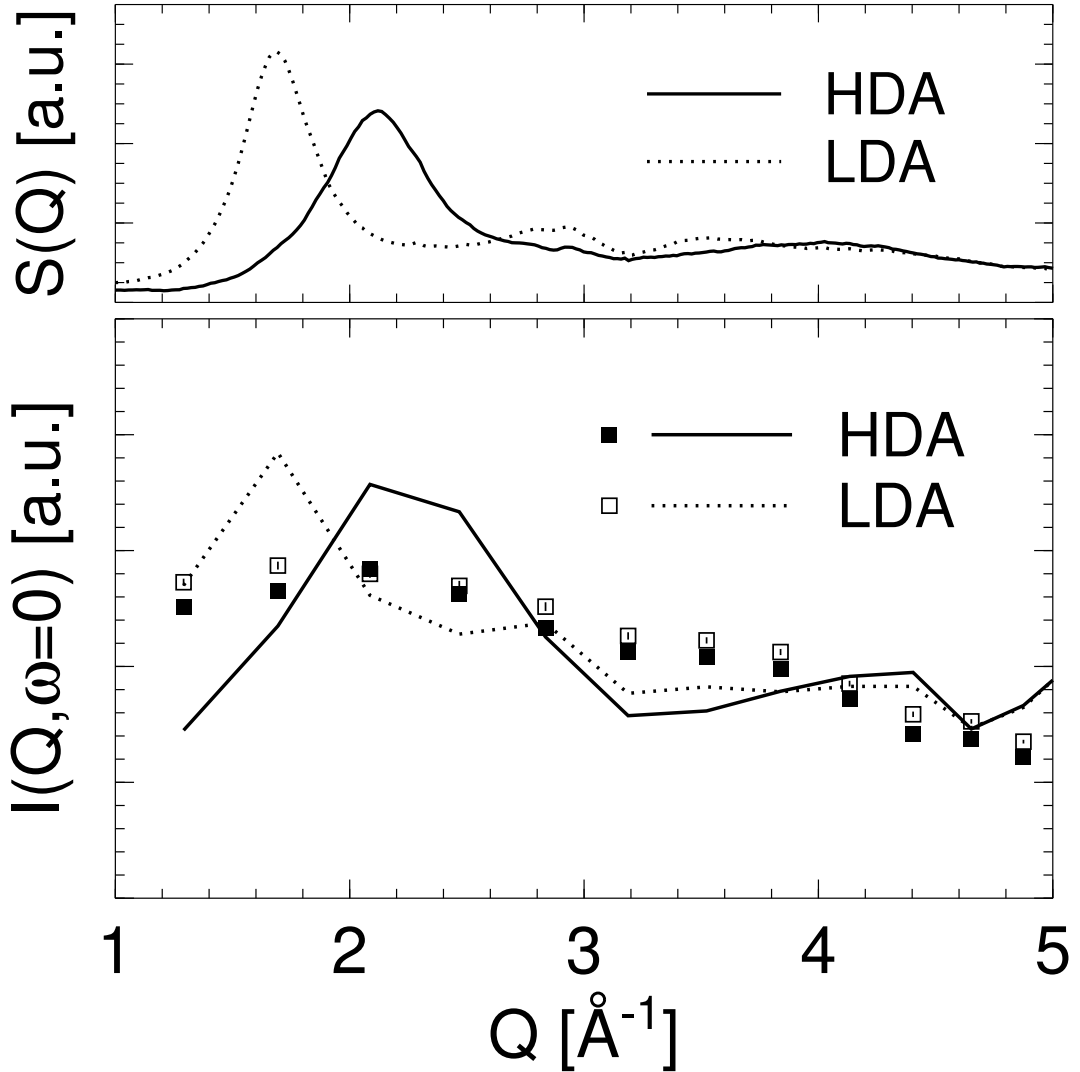


FIG. 1: Bottom: Elastic intensity $I(Q, \omega = 0)$ of the amorphous samples measured on the spectrometer IN13 at $T \approx 2$ K. Solid and dotted lines represent the HDA and LDA structures studied with the deuterated sample S2, respectively. ■ and □ represent the HDA and LDA structures studied with the partially protonated sample S1, respectively. Top: For comparison static structure factor of the deuterated HDA and LDA samples measured with high resolution on the diffractometer D20.

A more detailed introduction into this field can be found in textbooks on neutron scattering [62, 63, 64]. At the beginning we restrict our consideration to a harmonic system whose scattering characteristic is assumed to be isotropic. These terms are well met by amorphous solids. For such a system the intensity measured in an elastic scan mode neutron scattering

experiment can be written as

$$S(Q, \omega = 0) = \exp(W(Q, T)) \cdot S(Q) \quad (2)$$

$$W(Q, T) = -Q^2 \langle u^2(T) \rangle \quad (3)$$

with $W(Q, T)$ the Debye–Waller factor, $\langle u^2(T) \rangle$ the mean–square displacement of the scatterers, and $S(Q)$ the static structure factor, which may be approximated for incoherent scattering by a scaling factor $(2\pi N)^{-1}$ representing the number of scatterers in the sample [70]. Harmonicity implies that $\langle u^2(T) \rangle$ can be related to the density of states denoted as $G(\omega)$ as

$$\langle u^2(T) \rangle = \frac{1}{6} \frac{\hbar^2}{M} \int \frac{G(\omega)}{\hbar\omega} \coth\left(\frac{\hbar\omega}{2k_B T}\right) d\omega \quad , \quad (4)$$

M representing the mass of the scatterers [71]. Taking the low and high temperature limits into consideration $\langle u^2(T) \rangle$ can be asymptotically approximated by the moments of energy $\langle \omega^{-1} \rangle$ und $\langle \omega^{-2} \rangle$ as

$$\langle u^2(T \rightarrow 0) \rangle = \frac{\hbar^2}{6M} \cdot \int \frac{G(\omega)}{\hbar\omega} d\omega \quad , \quad (5)$$

$$\langle u^2(T \rightarrow \infty) \rangle = \frac{\hbar^2}{3M} \cdot k_B T \cdot \int \frac{G(\omega)}{\hbar^2 \omega^2} d\omega \quad . \quad (6)$$

As a consequence, the mean–square displacement is expected to cross over from a constant value at low temperatures to a $\propto T$ behaviour upon heating leading to the relation

$$W(Q, T) \propto -Q^2 \cdot T \quad . \quad (7)$$

Please note, that $\langle u^2(T \rightarrow 0) \rangle$ measured in neutron scattering experiments is not the absolute zero–point oscillation of the scatterers. Its value depends on the incident neutron energy. This energy sets a limit to the energy range on which the spectral density of the scatterers is sampled at $T \rightarrow 0$ K. However, $\langle u^2(T \rightarrow 0) \rangle$ denotes a well defined quantity which makes possible to draw comparative conclusions upon the properties of different sample states under identical experimental conditions.

Going back to eq. 2, we can quantitatively determine two physical effects which can induce changes in the observable elastic intensity $S(Q, \omega = 0)$. Firstly, the structure of the sample detectable as $S(Q)$ can change due to phase transformations. Secondly, the spectral density $G(\omega)$ can alter and influence both the low and high temperature properties of $S(Q, \omega)$ via eqs. 5 and 6, respectively. From the experimental point of view neutron scattering offers

the opportunity of discerning these two points by utilising, on the one hand, incoherent scatterers (protonated samples S1, S3 and S4) to study changes in $G(\omega)$ and, on the other hand, coherent scatterers (deuterated samples S2) to measure also changes in $S(Q)$.

Finally, utilising the Debye approximation for $G(\omega)$ [72]

$$G(\omega) = \frac{1}{2\pi^2} \cdot \frac{V}{N} \cdot \frac{3}{\bar{v}^3} \cdot \omega^2 \quad (8)$$

with \bar{v} the average velocity of sound

$$\frac{3}{\bar{v}^3} = \frac{1}{v_l^3} + \frac{2}{v_t^3} \quad (9)$$

the observables $G(\omega)$ and $\langle u^2(T) \rangle$ given in eqs. 5 and 6 can be compared qualitatively and quantitatively with results from other experimental techniques accessing the velocity of sound. Within the Debye model a characteristic quantity is the Debye temperature T_D

$$T_D^3 = 2\pi^2 \cdot \left(\frac{\hbar}{k_B} \right)^3 \cdot \frac{3sN}{V} \cdot \bar{v}^3 \quad , \quad (10)$$

with $3sN/V$ the density of vibrational modes of the system, which can be also extracted by numerical techniques from eq. 4 as

$$\langle u^2(T) \rangle = \frac{3}{2} \frac{\hbar^2}{Mk_B} \cdot \frac{T^2}{T_D^3} \cdot \int_0^{T_D/T} x \cdot \coth(x/2) \cdot dx \quad . \quad (11)$$

IV. RESULTS AND DISCUSSION

IV.a. Phase transformations and glass–transition

To give an overview on the temperature dependence of the elastic signal and its changes during the thermal treatment, Fig. 2 reports on the intensity $I(\omega = 0)$ measured in elastic scans with S1 on IN13 and S3 on IN16. $I(\omega = 0)$ is the intensity integrated over the accessible Q range of the instruments. The data sets are normalised to the intensity detected at $T = 2$ K in the crystalline cubic phase I_c (S1, IN13) and LDA (S3, IN16). The phase transformations HDA \rightarrow LDA and LDA \rightarrow I_c can be identified in both samples as rather sharp intensity gains in the elastic response at $T \approx 110$ K and $T \approx 150$ K. They are

indicated by vertical arrows. Additionally, a small step in intensity at $T \approx 240$ K indicates the formation of the hexagonal crystal from ice I_c as reported in reference [16, 73].

At sufficiently high T (≥ 40 K), the intensity of all phases decreases linearly upon heating in the logarithmic presentation of Fig. 2. This behaviour is stressed by solid lines. Neither in the T range of HDA \rightarrow LDA nor in the T regime of the LDA \rightarrow I_c and, thus, the assumed glass–transition, a pronounced drop off in $I(\omega = 0)$ can be detected. Such a drop off would be a mandatory fingerprint for an enhancement in molecular mobility of the sample (eq. 2) on time scales less than a few nano–seconds.

A missing enhancement in molecular mobility is also confirmed by energy scan measurements with the incoherently scattering sample S4 on IN16. Spectra measured at different temperatures are reported in Fig. 8. To compensate for the here nonrelevant temperature dependence of the elastic intensity the data are normalised to the maximum intensity at the respective temperatures. The identity of all spectra demonstrates that within the instrumental resolution of 1 μ eV no relaxation processes are present in the sample. From the comparison of the different data to the results measured at 2 K it is evident that the spectra do not change markedly their shape in the energy window of ± 10 μ eV, regardless of the state of the sample (The contribution of phonons in this energy window is too weak to leave a trace in the temperature dependence.) In accordance with the IN16 data, no change of the inelastic response apart from the normal harmonic phonon contribution can be observed in the IN6 experiments at temperatures prior to the recrystallisation of the amorphous samples. We may conclude that according to eqs. 2 and 3 there is no evidence for a development of additional decay channels for the elastic intensity at the assumed glass transition with $T_g \approx 135$ K. There is no evidence of relaxation behaviour in the course of the transformations HDA \rightarrow LDA and LDA \rightarrow I_c, either. Consequently, the presence of relaxation processes like translational diffusion over intermolecular distances on a time scale shorter than some nano–seconds can be excluded.

Before we will discuss the Debye–Waller factor in detail and, thus, the potential relaxation processes on shorter length scales, it is important to establish the regime of stability of the amorphous structures. We focus here primarily on the supposed glass transition and the LDA \rightarrow I_c transformation. Fig. 4 reports on the elastic intensity $I(Q, \omega = 0)$ measured with S2 on IN13 at different temperatures which correspond to the regime of the glass transition. The temperatures are indicated by vertical arrows in Figure 4 c. Here, $I(Q, \omega = 0)$ is

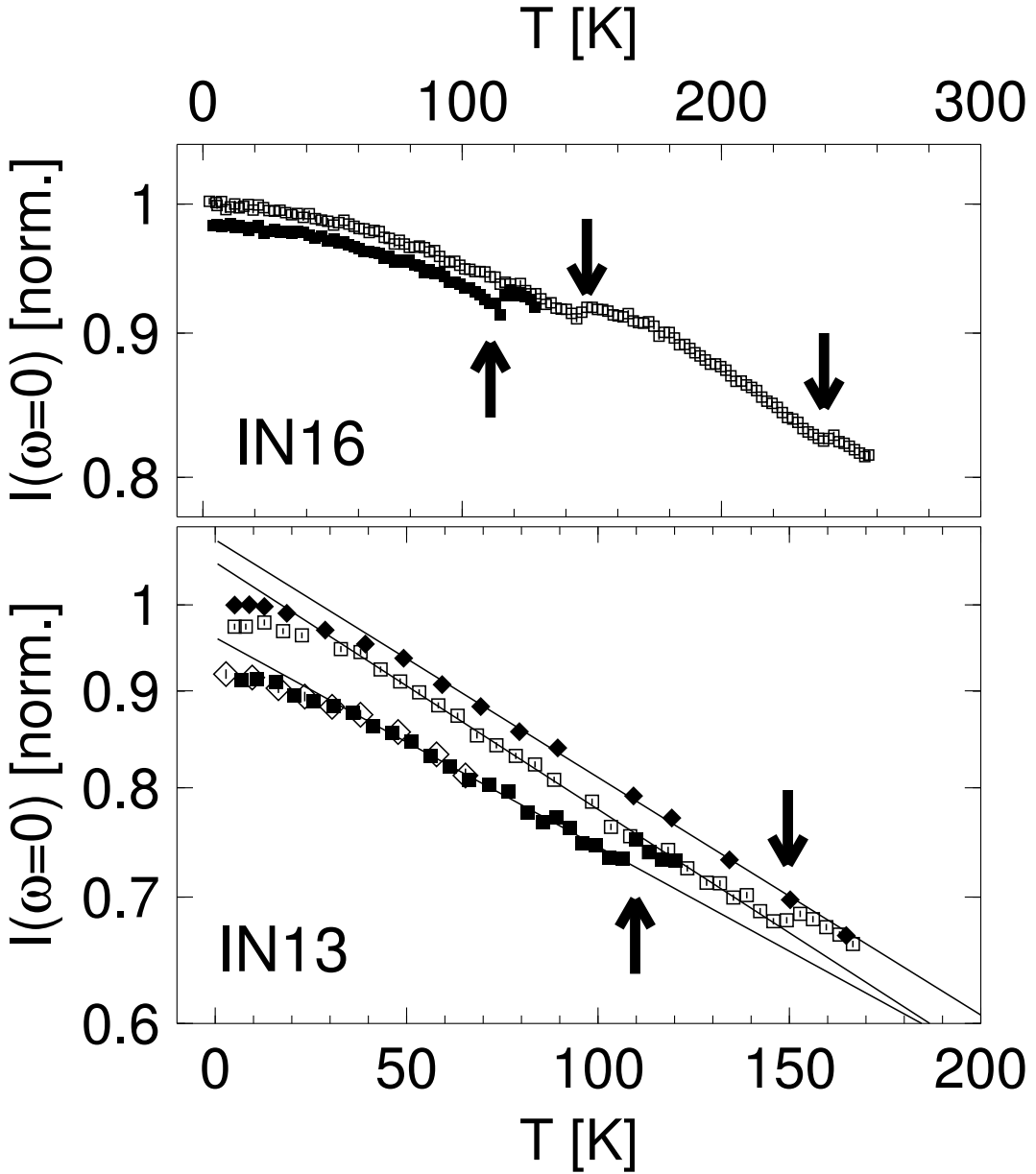


FIG. 2: Temperature dependence of the elastic intensity $I(\omega = 0)$ measured with the partially protonated sample S1 on IN13 and the fully protonated sample S3 on IN16. The signal is integrated over the accessible Q -range of the instruments. Data on HDA are represented as \diamond (IN13) and \blacksquare (IN13 and IN16), on LDA as \square (IN13 and IN16), and on cubic ice I_c as \blacklozenge . Details on the thermal treatment of the samples are given in the text. The intensity is normalised to the $I(\omega = 0)$ at $T \approx 2$ K of I_c on IN13 and of LDA on IN16. Upward arrows indicate the transformation HDA \rightarrow LDA at $T \approx 110$ K, downward arrows indicate the transformation LDA \rightarrow I_c at $T \approx 150$ K and from cubic to hexagonal ice at $T \approx 240$ K measured on IN16 exclusively. Solid lines stress the linear behaviour of the intensity expected for a harmonic solid at sufficiently high temperature.

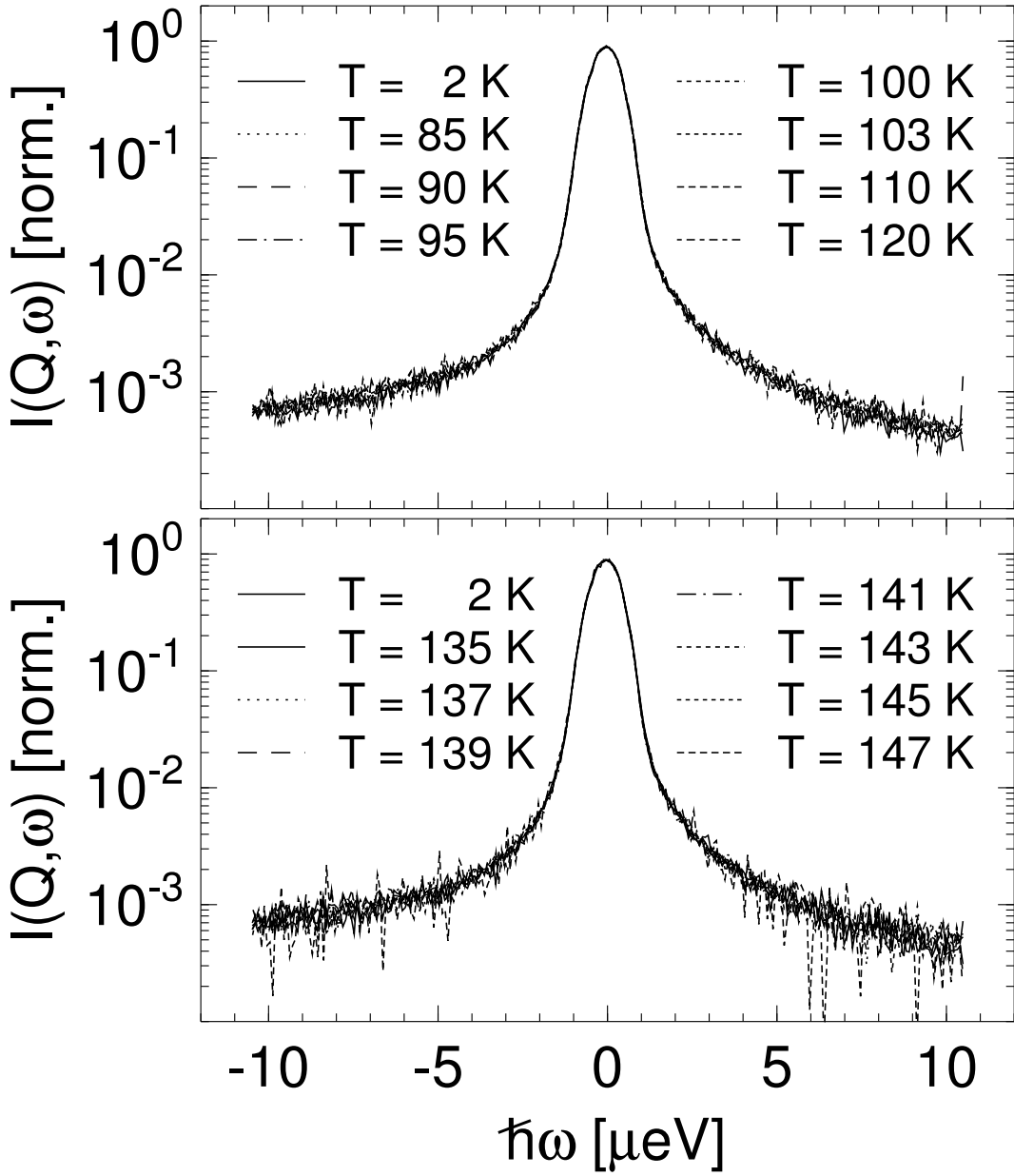


FIG. 3: Energy scans $I(Q, \omega)$ of the fully protonated sample S4 measured on IN16. All spectra are normalised to the maximum intensity determined at the respective temperatures that are indicated in the figures. Top figure reports spectra measured in the course of the HDA \rightarrow LDA transformation, bottom figure reports spectra measured in the temperature range of the apparent glass transition. Also plotted are data obtained at $T \approx 2$ K representing the instrumental resolution. Please note, that there is no difference between the $I(Q, \omega)$ at different temperatures.

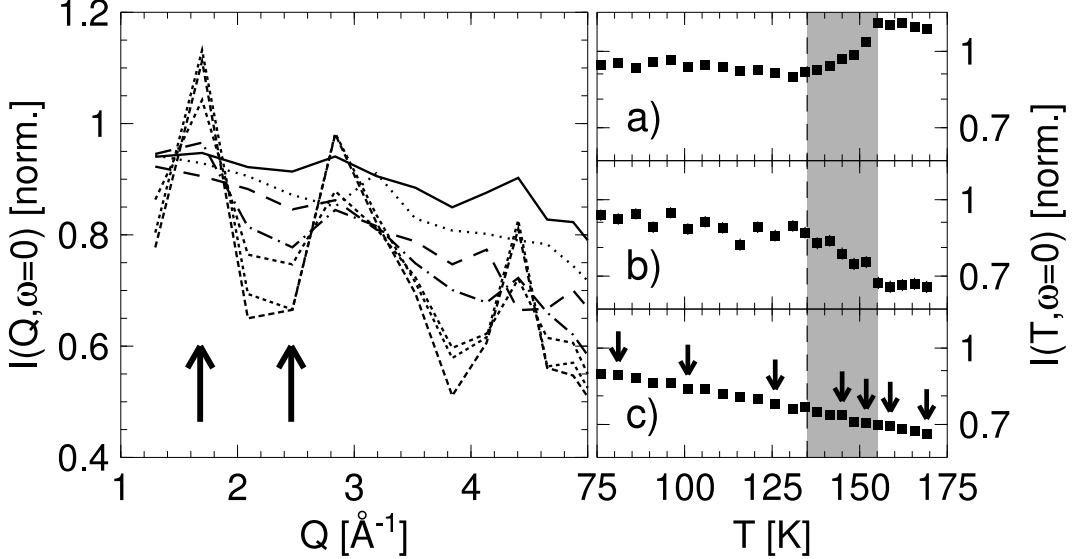


FIG. 4: Left: Temperature evolution of the elastic intensity $I(Q, \omega = 0)$ during the transformation of LDA into ice I_c measured on the spectrometer IN13 between $T \approx 80$ K and $T \approx 170$ K. The nominal temperatures are indicated by arrows in figure c in the right panel. The two arrows indicate the Q -values at which the temperature dependence $I(T, \omega = 0)$ is inspected in detail in figures a and b in the right panel. Right: Elastic intensity $I(T, \omega = 0)$ measured at $Q = 1.7 \text{ \AA}^{-1}$ in figure a, at $Q = 2.4 \text{ \AA}^{-1}$ in figure b, and integrated over the accessible Q -range in figure c. Dashed vertical line stresses the supposed glass transition and the grey shaded area indicates the transition regime of LDA to ice I_c

normalised to $I(Q, \omega = 0)$ of LDA determined at 2 K. It gives, therefore, the relative changes before and after the conversion of LDA into I_c . The two arrows indicate the Q values at which the temperature dependent intensity $I(T, \omega = 0)$ is plotted in Figure 4 a and b. As it is expected from a harmonic system $I(Q, \omega = 0)$ exhibits up to 130 K only a loss of intensity due to the Debye–Waller factor (eq. 3). Whereas at 170 K $I(Q, \omega = 0)$ shows a detailed Q -dependence arising from changes in $S(Q)$ (eq. 2). The sharp maxima are Bragg–reflections of crystalline cubic ice as it is presented in detail in reference [65].

The temperature dependence of the elastic intensity $I(T, \omega = 0)$ is reported in the right panel of Fig. 4. Plotted data are taken at $Q = 1.7 \text{ \AA}^{-1}$ (Fig. 4 a) and $Q = 2.4 \text{ \AA}^{-1}$ (Fig. 4 b). Figure 4 c shows the signal integrated over the accessed Q range. It is evident from Figure 4 c that despite the intensity gain at the Bragg reflections (Fig. 4 a) and

intensity loss between (Fig. 4 b) the total scattering power in the accessed Q range does not show any anomalies in the temperature range of the supposed glass transition. In conclusion, the behaviour of $I(T, \omega = 0)$ in Fig. 4 gives evidence of a redistribution of the signal within the elastic channel only, which is compatible with a recrystallisation of the LDA matrix. This recrystallisation is obviously slow at $T < 150$ K but very efficient above 150 K [74, 75], causing the rapid gain in $I(\omega = 0)$ shown in Fig. 2. The very onset of the recrystallisation matches with the supposed glass transition temperature $T_g \approx 135$ K that is indicated by the dashed vertical line in Figure 4.

IV.b. Debye–Waller factor and mean–square displacement

As it is outlined in section III the Debye–Waller factor $W(Q, T)$ of a harmonic system obeys the simple relation $W(Q, T) \propto -T \cdot Q^2$. Figures 5 and 6 show the T – and the Q^2 –dependence of some selected $W(Q, T)$ data sets for the samples S1 and S2 measured on IN13. Since, the zero point oscillation of the scatterers is of no importance for the discussion of $W(Q, T)$ here, the presented data sets are normalised to the signals measured at 2 K. It is obvious from Fig. 5 that all phases, HDA, LDA, and ice I_c, display a Q^2 –dependence and are (meeting the requirement of sufficiently high temperature) proportional to T . The linearity in T is equally fulfilled for the elastic intensity of S2 plotted in Fig. 6 up to temperatures close to the transformations of the phases. Grey shaded areas in Fig. 6 indicate the transformation regions, in which the structural correlations change, as it is shown in Fig. 4. The Q^2 –dependence is as well fulfilled for HDA and LDA in S2 as it is for HDA, LDA and I_c in S1, which is demonstrated by fits plotted as solid lines in Figs. 5 and 6.

According to eq. 3 the slopes of the fits correspond to the mean–square displacement $\langle u^2(T) \rangle$ of the scatterers. They are shown for both S1 and S2 in Fig. 7. Despite the different levels of deuteration of S1 and S2 the $\langle u^2(T) \rangle$ of both samples in the HDA and LDA states are comparable. Please note that the onset of structural changes, which the samples encounter during the phase transitions, is demonstrated by the strong enhancement of statistical uncertainty. The comparable $\langle u^2(T) \rangle$ values of both samples in the corresponding phases can be understood when taking into consideration that at the exploited temperatures $\langle u^2(T) \rangle$ is strongly influenced by the mean velocity of sound (eq. 9). It has been shown that

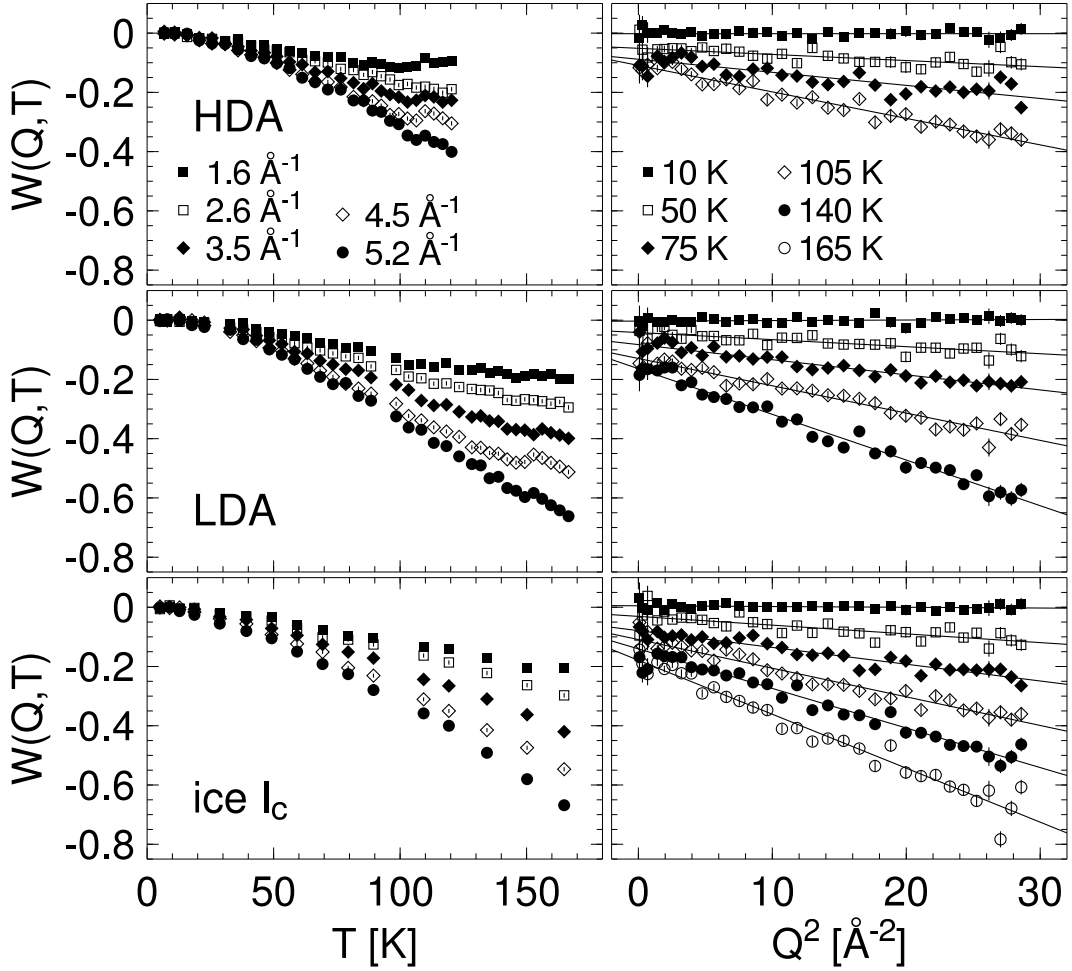


FIG. 5: Debye–Waller factor $W(Q, T)$ of HDA, LDA and ice I_c measured with the partially protonated sample S1 on IN13. Left panel gives the temperature dependence of $W(Q, T)$, right panel gives the Q –dependence of $W(Q, T)$ plotted vs. Q^2 to stress the behaviour expected for a harmonic solid. The selected Q –values and approximate temperatures valid for all presented data are given in the top subfigures. Solid lines correspond to Q^2 –fits to the data whose slope is interpreted as the mean–square displacement $\langle u^2(T) \rangle$ in Fig. 7.

for the crystalline hexagonal ice I_h the level of deuteration does not change markedly the elastic constants or thermodynamic observables being determined by the vibrational properties [2, 76, 77]. This means that the velocity of sound does not alter strongly with the level of deuteration. For example, a difference of only 3% was found in specific heat measurements of crystalline ice at $T \leq 70$ K as an effect of deuteration [77]. A similar behaviour can be expected in the phases studied here.

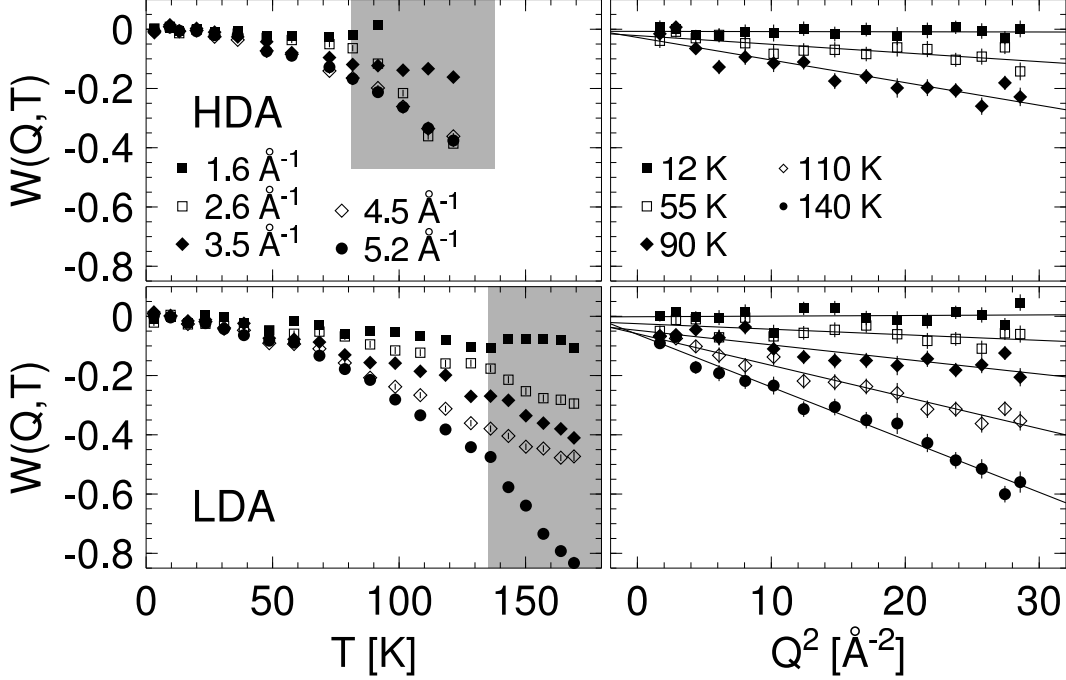


FIG. 6: Debye–Waller factor $W(Q, T)$ of HDA and LDA measured with the deuterated sample S2 on IN13. Left panel gives the temperature dependence of $W(Q, T)$, right panel gives the Q –dependence of $W(Q, T)$ plotted vs. Q^2 to stress the linear behaviour expected for a harmonic solid. The selected Q –values and approximate temperatures valid for all shown data are given in the top subfigures. Solid lines correspond to Q^2 –fits to the data whose slope is interpreted as the mean–square displacement $\langle u^2(T) \rangle$ in Fig. 7. Please note that original data have been grouped by having summed up two data points each.

Assuming that the Debye model is applicable a Debye temperature T_D can be extracted from fits to $\langle u^2(T) \rangle$ via eq. 11. Fit results are plotted as solid (S1) and dotted (S2) lines in Fig. 7 and the obtained T_D are given in Table II. The upper fitting limits are given by the transition temperatures which are obtained with sample S2 and shown in Fig. 6.

Another observable in neutron scattering from which $\langle u^2(T) \rangle$ can be calculated is the density of states $G(\omega)$ (eq. 4). Figure 8 reports $G(\omega)$ measured on the time–of–flight spectrometer IN6 [44, 45, 46]. The plotted $G(\omega)$ are calculated from data measured at 80 K (HDA), 127 K (LDA) and 160 K (ice I_c). Within the statistical accuracy of the measurements performed at different T no deviations from the presented $G(\omega)$ could have been established. A self consistent multi–phonon calculation was applied to the data in addition

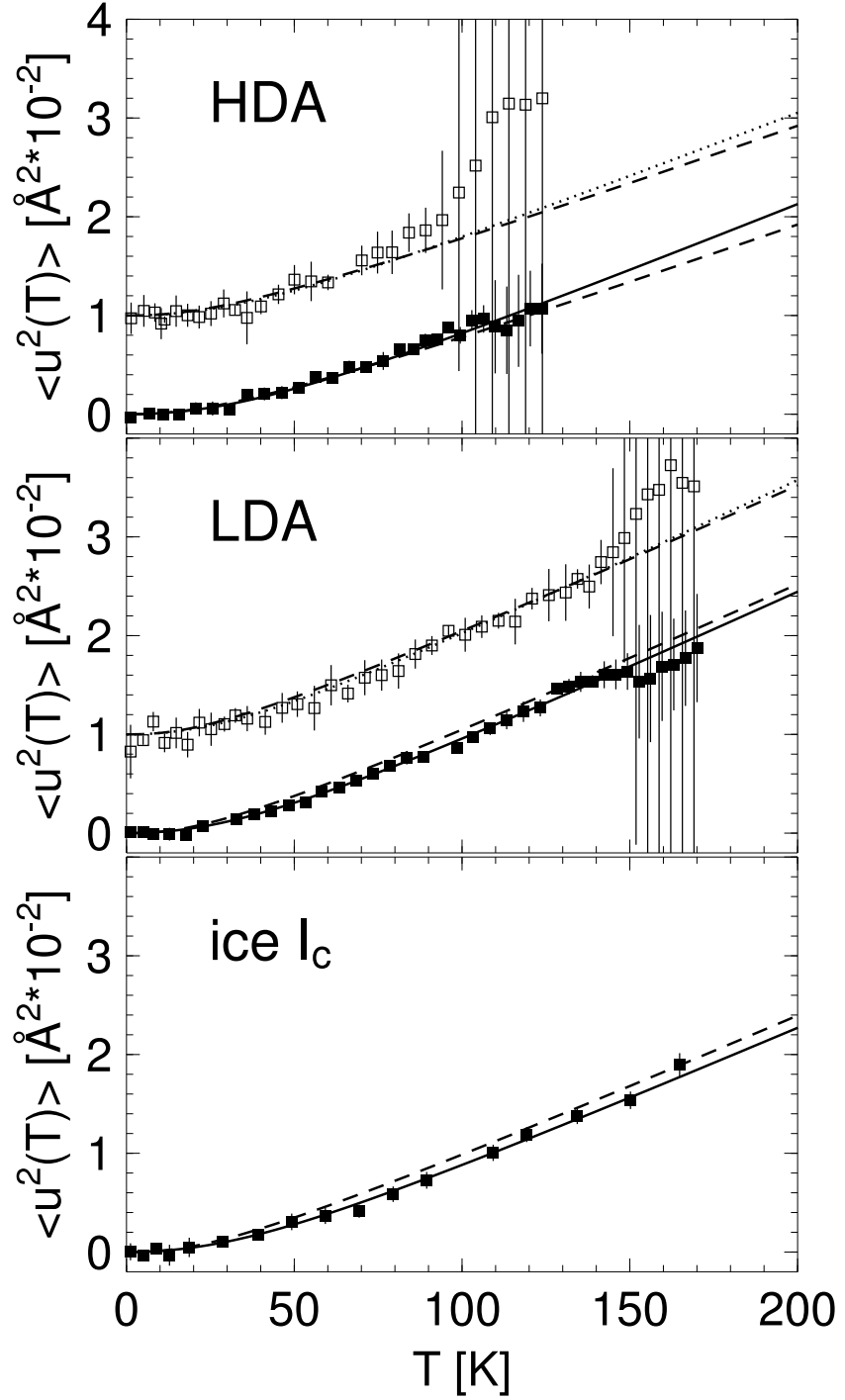


FIG. 7: Mean-square displacement $\langle u^2(T) \rangle$ of HDA, LDA and ice I_c determined from data taken with sample S1 (■) and with sample S2 (□) shown in Figs. 5 and 6, respectively. Solid lines correspond to fits with the Debye-model to data taken on S1, dotted lines correspond to fits to data on S2. Dashed lines are calculated with eq. 4 from the generalised density of states given in Fig. 8. Please note that data of sample S2 have been shifted for a better visibility.

TABLE II: Debye–temperatures T_D obtained from fits to the data shown in Fig. 7 and estimated from velocity of sound given in [83].

phase	sample S1	sample S2	from [83]
HDA	230 ± 6 K	223 ± 9 K	230 K
LDA	217 ± 2 K	202 ± 3 K	203 K
ice I _c	224 ± 7 K	–	203 K

to the standard correction procedures [44, 78].

Since the data are obtained with a fully deuterated, coherently scattering sample the determined $G(\omega)$ is an approximation to the true density of states [79, 80, 81]. To account for the perturbations by the coherent scattering a correction factor $\alpha = 0.7$ is introduced. This factor is estimated independently comparing $G(\omega)$ of hexagonal ice I_h and ice XII measured on fully deuterated and fully protonated samples [82]. The Debye levels of the samples are indicated in Fig. 8 and compared to the Debye levels obtained in ultrasonic experiments on ice I_c [83] and Brillouin light scattering on ice I_h [84], both techniques giving comparable values. Taking α and $G(\omega)$ from Fig. 8 into account, a $\langle u_{G(\omega)}^2(T) \rangle$ is calculated to the values presented as dashed lines in Fig. 7.

Within the statistics of the measurements and the accuracy of the applied data analysis the results obtained from backscattering and time–of–flight measurements fully agree. For example, in the framework of the Debye model both techniques indicate the highest average velocity of sound and, thus, the highest T_D for HDA. Debye temperatures estimated via eq. 10 from results based on supersonic measurements [83] are included in Table II and their respective Debye levels for $G(\omega)$ are indicated in Fig. 8. Although obtained with a different technique the T_D match nicely the values observed in our elastic neutron scattering experiments giving also a higher value for T_D for HDA [85].

We would like to recall the fact that the coherent character of the sample introduces uncertainties into $G(\omega)$ although these are well controlled [82]. Thus, the excellent agreement of $\langle u_{G(\omega)}^2(T) \rangle$ with $\langle u^2(T) \rangle$ calculated from the Debye–Waller factor $W(Q, T)$ should not be over-interpreted. However, qualitatively the results on $W(Q, T)$ and $\langle u^2(T) \rangle$, which are determined by studying the elastic signal, and, on the other hand, the data on $\langle u_{G(\omega)}^2(T) \rangle$, which is obtained from the inelastic response, give a coherent picture of the properties of

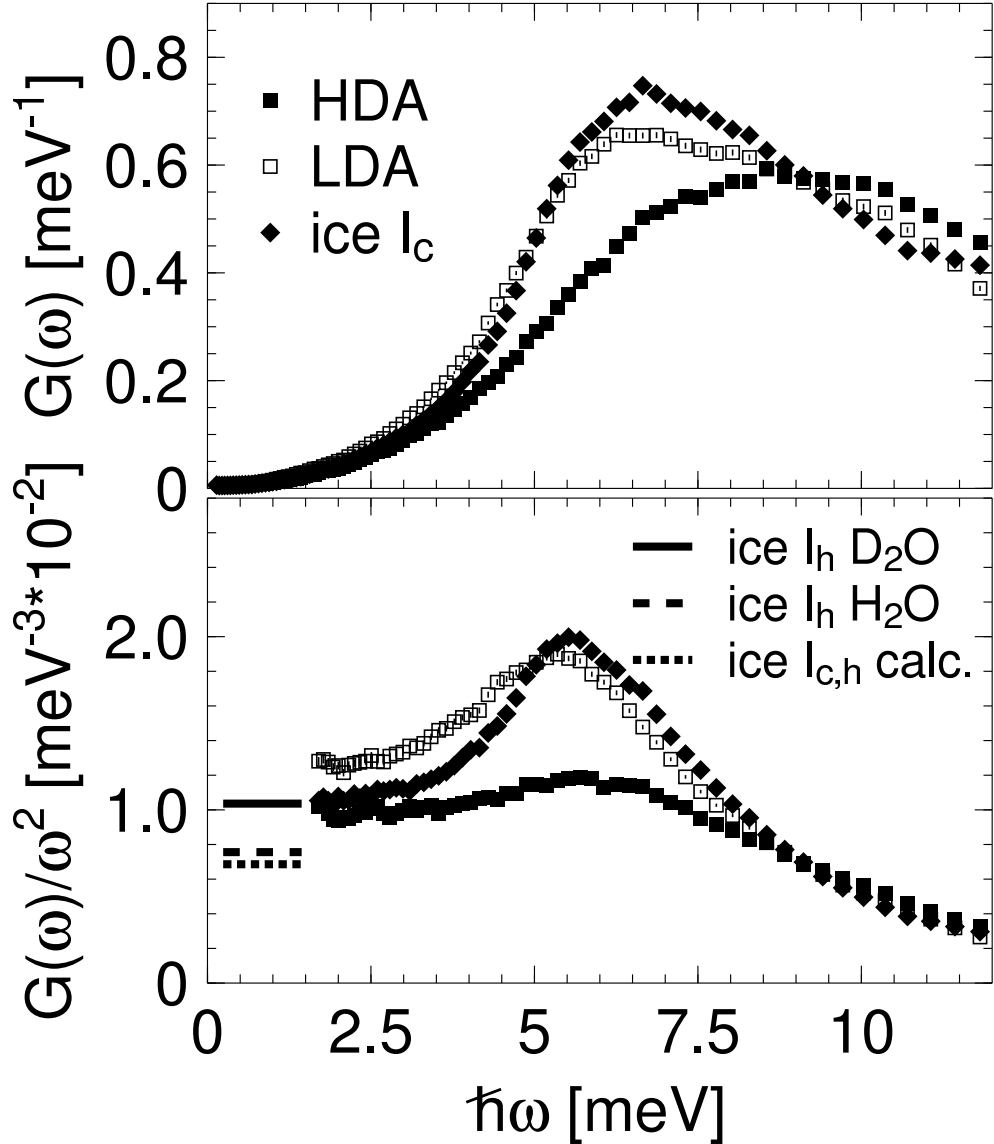


FIG. 8: Top: Generalised density of states $G(\omega)$ of HDA (■), LDA (□) and ice I_c (♦) determined on the time-of-flight spectrometer IN6 on a fully deuterated sample. All $G(\omega)$ are normalised to 12 modes in the energy range $\hbar\omega \leq 40$ meV. Bottom: $G(\omega)/\omega^2$ emphasises the low energy range where a constant value is expected for harmonic solids. Please note that data at $\hbar\omega \leq 1.5$ meV are perturbed by the resolution of the spectrometer and therefore suppressed in the figure. Equally shown are the Debye-levels determined independently for fully deuterated (solid line) and fully protonated (dashed line) ice I_h , from which a factor of 0.7 accounting for the coherency effect is estimated. Dotted line represents Debye-levels calculated from [83] for ice I_c and from [84] for ice I_h obtained by ultrasonic and light scattering experiments, respectively.

HDA, LDA and ice I_c. They mark them unequivocally as harmonic systems.

Finally, we discuss the Debye temperatures determined by specific heat measurements [16] as 288 K for HDA, 305 K for LDA and 325 K for ice I_h. The fundamental difference is that T_D is determined here for $T \ll T_D$, i.e. within the validity limits of the Debye model. For this range specific heat measurements on ice I_h give T_D values of about 200 K with a difference of less than 3 % at $T < 70$ K between deuterated and protonated samples [77], as it was already indicated above. At elevated temperatures the specific heat reflects the details of the phonon density of states $G(\omega)$ beyond the acoustic region and the extracted T_D becomes temperature dependent [72]. Taking only translational modes, i.e. phonons, into consideration the T_D of ice I_h reaches a maximum at $T \approx 100$ K with $T_D \approx 300$ K [77]. Consequently, the basic difference of about 100 K between the T_D presented here and cited in [16] is due to the applied experimental techniques and the thermodynamic conditions of the measurements, but the data do agree in the general concept of harmonic solids [64, 72].

The low value of T_D of HDA given in [16] can be, on the one hand, understood by the temperature sensitivity of T_D in the specific heat measurements. At about 100 K not only phonons but also librations contribute to $C_p(T)$ [44, 77, 82]. It is well established by experiments that the librational band shifts toward lower energies the higher the density of the ice phase is. The shift of the librational band in HDA raises the specific heat and consequently pulls T_D below the value of crystalline ice [44, 46, 86]. This effect is well comparable with the issue of deuteration a crystalline sample [44, 77]. On the other hand, it must be stressed that the sample referred to as HDA in [16] was annealed before the measurements raising the question of the sample state. In the case of a mixture of HDA-type and LDA-type phases or even a contribution of ice XII [25, 67, 82] the density of states would decrease T_D more efficiently when increasing T .

VI.c. Excess of modes at low T

So far we have not discussed the zero point oscillation of the scatterers in HDA, LDA and ice I_c which is indicated in Fig. 2. Indeed, bearing in mind that the elastic intensity is coupled to the inelastic response (eqs. 2, 3, 4, 5) there is an inconsistency concerning the behaviour of HDA. Since, among all phases the lowest Debye-level is detected for HDA (Fig. 8), it strictly requires the highest elastic intensity $I(\omega = 0)$ at $T \approx 0$ K. However,

HDA exhibits the lowest $I(\omega = 0)$ measured in all our experiments (Fig. 2). It must be notified that this inconsistency with $I(\omega = 0)$ holds also for results from other experiments exploiting the dynamic response of the phases [43, 46, 55, 83].

Moreover, the Debye–Waller factors $W(Q, T)$, the mean–square displacements $\langle u^2(T) \rangle$, and the Debye temperatures T_D calculated from the elastic scan measurements itself display a dependence on temperature which is in full agreement with the $G(\omega)$ determined by time–of–flight techniques. Consequently, the temperature evolution of the elastic intensity $I(\omega = 0, T)$ of HDA contradicts its own value at very low temperatures $I(\omega = 0, T \rightarrow 0)$.

This self–contradicting behaviour of HDA can be resolved, if not only phonons, i.e. excitations following the Bose statistics, are inherent to the dynamic response but also non–Bose modes predominant at low temperatures are present. Such modes have been detected for the first time by three axis neutron scattering (TAS) [53, 54], confirmed later and interpreted as the contribution of two–level systems (TLS) to the inelastic response of HDA [48, 49, 50, 52]. Remarkably, no TLS are observed in the LDA state. Please note, that the level of deuteration of the sample has no significant influence on the TLS intensity [48, 49, 87].

V. SUMMARY AND CONCLUSIONS

We utilised the neutron back–scattering and time–of–flight techniques to gain information on the temperature dependence of the high–density (HDA) and low–density (LDA) amorphous states of ice and the crystalline phase I_c . Particular focus was put on the phase transformations $HDA \rightarrow LDA$, $LDA \rightarrow I_c$ and the supposed glass–transition of LDA with $T_g \approx 135$ K, the mean–square displacements of the scatterers in the stable states HDA, LDA and I_c , and their relative zero point oscillations.

Within the best energy resolution of $1 \mu\text{eV}$ of the experiments no relaxation processes, giving evidence of a higher mobility of the scatterers, can be identified during the phase transformations. From results on coherently scattering samples, we may conclude that at or prior to $T \approx 135$ K, i.e., at the very T_g discussed in literature, the recrystallisation of LDA into I_c sets in – thus preventing any data analysis in terms of Mode Coupling Theory as it is outlined in [65].

The temperature and Q –dependence of the Debye–Waller factors and the resulting mean–

square displacements mark HDA, LDA and ice I_c as harmonic solids. In the framework of the Debye model HDA reveals a higher Debye temperature, a higher average velocity of sound, and thus a lower phonon density of states at low energy when compared with LDA and ice I_c. LDA and ice I_c show rather similar dynamic properties. The conclusions drawn from the elastic scan data on the temperature dependence of all states are in full agreement with results obtained by other experimental techniques.

The relative elastic intensities determined at low temperatures support the existence of additional modes in HDA not obeying the Bose statistics, i.e. this excess should not be confused with a Boson-peak as it is identified in glassy systems [41]. These modes have been observed in inelastic neutron scattering [53, 54], confirmed and interpreted as two-level systems from light absorption experiments [48, 49, 50].

In the case of the protonated samples, the scattering from hydrogen is by a factor of ~ 40 stronger than the scattering from oxygen. Consequently, the signal measured with samples S3 and S4 is not only determined by the dynamic properties of the water molecules but equally reflects the characteristics of the hydrogen sublattice. The absence of anomalies in the Debye-Waller factor excludes therefore any strong proton relaxation within the matrix. However, migration of lattice defects, as discussed in references [35, 36, 37], is not detectable due to their too low concentration.

ACKNOWLEDGEMENTS:

We wish to thank D.D. Klug and N.I. Agladze for helpfull discussions.

- [1] P.V. Hobbs, *Ice Physics*, Claredon Press Oxford, (1974).
- [2] V.F. Petrenko, and R.W. Whitworth, *Physics of ice*, Oxford University Press, (1999).
- [3] O. Mishima, L.D. Calvert and E. Whalley, *Nature*, **310**, 393 (1984).
- [4] O. Mishima, L.D. Calvert and E. Whalley, *Nature*, **314**, 76 (1985).
- [5] P.H. Poole, U. Essmann, F. Sciortino, and H.E. Stanley, *Phys. Rev. E*, **48**, 4605, (1993).
- [6] P.H. Poole, F. Sciortino, T. Grande, H.E. Stanley and C.A. Angell, *Phys. Rev. Lett.*, **73**, 1632, (1994).

[7] P.G. Debenedetti, *Metastable Liquids – Concepts and Principles*, Princeton University Press, 1996.

[8] O. Mishima and H.E. Stanley, *Nature*, **396**, 329, (1998).

[9] H.E. Stanley, S.V. Buldyrev, M. Canpolat, O. Mishima, M.R. Sadr-Lahijanin, A. Scala and F.W. Starr, *Phys. Chem. Chem. Phys.*, **2000**, 1551, (2000).

[10] A.H. Narten, C.G. Venkatesh, and S.A. Rice, *J. Chem. Phys.*, **64**, 1106, (1976).

[11] E. Mayer, and P. Brueggeller, *Nature*, **298**, 5876, (1982).

[12] E. Mayer, and R. Pletzer, *J. Chem. Phys.*, **80**, 2939, (1983).

[13] O. Mishima, and Y. Suzuki, *J. Chem. Phys.*, **115**, 4199, (2001).

[14] Please note that structures obtained by vapour deposition and hyper-quenching at ambient pressure, which are often referred to as ASW and HGW in literature, are comparable to the structure of the LDA phase [15]. Since our study is focussed on LDA exclusively, we refer to other low-density amorphous states as LDA-type phases or LDA-type structures.

[15] M.C. Bellissent-Funel, L. Bosio, A. Hallbrucker, E. Mayer, and R. Sridi-Dorbez, *J. Chem. Phys.*, **97**, 1282, (1992).

[16] Y.P. Handa, O. Mishima and E. Whalley, *J. Chem. Phys.*, **84**, 2766, (1986).

[17] G.P. Johari, A. Hallbrucker and E. Mayer, *Nature*, **330**, 552, (1987).

[18] Y.P. Handa and D.D. Klug, *J. Phys. Chem.*, **92**, 3323, (1988).

[19] A. Hallbrucker, E. Mayer, and G.P. Johari, *J. Phys. Chem.*, **93**, 7751, (1989).

[20] A. Hallbrucker, E. Mayer, and G.P. Johari, *Phil. Mag. B*, **60**, 179, (1989).

[21] G.P. Johari, A. Hallbrucker and E. Mayer, *J. Chem. Phys.*, **92**, 6742, (1990).

[22] G.P. Johari, A. Hallbrucker and E. Mayer, *J. Phys. Chem.*, **94**, 1212, (1990).

[23] E. Mayer, *J. Mol. Struc.*, **250**, 403, (1991).

[24] G.P. Johari, A. Hallbrucker and E. Mayer, *J. Chem. Phys.*, **95**, 6849, (1991).

[25] C.G. Salzmann, I. Kohl, T. loerting, E. Mayer, and A. Hallbrucker, *Phys. Chem. Chem. Phys.*, **5**, 3507, (2003).

[26] O. Mishima, *J. Chem. Phys.*, **121**, 3161, (2004).

[27] C.A. Angell and W. Sichina, *Ann. N.Y. Acad. Sci.*, **279**, 53, (1976).

[28] C.A. Angell, *Chem. Rev.*, **102**, 2627, (2002).

[29] R.S. Smith, and B.D. Kay, *Nature*, **398**, 788, (1999).

[30] R.S. Smith, Z. Dohnalek, G.A. Kimmel, K.P. Stevenson, and B.D. Kay, *Chem. Phys.*, **258**,

291, (2000).

- [31] Y.P. Handa, D.D. Klug, and E. Whalley, *J. de Physique*, **48**, C1–435, (1987).
- [32] Y.P. Handa, D.D. Klug, and E. Whalley, *Can. J. Chem.*, **66**, 919, (1988).
- [33] O. Yamamuro, M. Oguni, T. Matsuo, and H. Suga, *J. Phys. Chem. Solids*, **48**, 935, (1987).
- [34] A.A. Tsekouras, M.J. Iedema, and J.P. Cowin, *Phys. Rev.—Lett.*, **80**, 5798, (1998).
- [35] M. Fischer, and J.P. Devlin, *J. Phys. Chem.*, **99**, 11584, (1995).
- [36] F. Fujara, S. Wefing, and W.F. Kuhs, *J. Chem. Phys.*, **88**, 6801, (1988).
- [37] T.M. Kirschgen, M.D. Zeidler, B. Geil, and F. Fujara, *Phys. Chem. Chem. Phys.*, **5**, 5247, (2003).
- [38] V. Velikov, S. Borick and C.A. Angell, *Science*, **294**, 2335, (2001).
- [39] G. Johari, *J. Chem. Phys.*, **119**, 2935, (2003).
- [40] Y.Z. Yue and C.A. Angell, *Nature*, **427**, 6976, (2004).
- [41] A.P. Sokolov, R.Calemzuk, B. Salce, A. Kisliuk, D. Quitmann and E. Duval, *Phys. Rev. Lett.*, **78**, 2405, (1997).
- [42] F. Sette, M.H. Krisch, C. Masciovecchio, G. Ruocco, and G. Monaco, *Science*, **280**, 1550 (1998).
- [43] H. Schober, M.M. Koza, A. Tölle, C. Masciovecchio, F. Sette and F. Fujara, *Phys. Rev. Lett.*, **85**, 4100, (2000).
- [44] M.M. Koza, *Studium der statischen und dynamischen Eigenschaften amorpher und kristalliner Wasserphasen und ihrer Phasenumwandlungskinetik*, PhD, Technische Universität Darmstadt, (2001).
- [45] M.M. Koza, *Report on the preparation and performance of time-of-flight experiments on the amorphous and polycrystalline solid D₂O*, Institut Laue Langevin, No.ILL97KO10T, (1997).
- [46] H. Schober, M. Koza, A. Tölle, F. Fujara, C.A. Angell and R. Böhmer, *Physica B*, **241–243**, 897, (1998).
- [47] O. Yamamuro, Y. Madokoro, H. Yamasaki, and T. Matsuo, *J. Chem. Phys.*, **115**, 9808, (2001)
- [48] N.I. Agladze and A.J. Sievers, *Phys. Rev. Lett.*, **80**, 4209, (1998);
- [49] N.I. Agladze and A.J. Sievers, *Europhys. Lett.*, **53**, 40, (2001);
- [50] N.I. Agladze and A.J. Sievers, *Physica B*, **316–317**, 513, (2002).
- [51] O. Andersson and H. Suga, *Phys. Rev. B*, **65**, 14020(R), (2002).
- [52] J.S. Tse, D.D. Klug, C.A. Tulk, E.C. Svensson, and J. Swainson, *Phys. Rev. Lett.*, **85**, 3185,

(2000).

[53] E.C. Svensson, W. Montfrooij, V.F. Sears, and D.D. Klug, *Physica B*, **316-317**, 513. (2002).

[54] C.A. Tulk, D.D. Klug, E.C. Svensson, V.F. Sears, and J. Katsaras, *Appl. Phys. A*, **74**, S1185, (2002).

[55] M.M. Koza, H. Schober, B. Geil, M. Lorenzen, and H. Requardt, *Phys. Rev. B*, **69**, 024204, (2004).

[56] G.P. Johari, *Chem. Phys. Phys. Chem.*, **2**, 1567, (2000).

[57] G. Tarjus, C. Alba-Simionescu, M. Grousson, P. Viot, and D. Kivelson, *J. Phys.: Cond. Matter*, **15**, 1077, (2003).

[58] J.S. Tse, D.D. Klug, C.A. Tulk, I. Swainson, E.C. Svensson, C.-K. Loong, V. Shpakov, V.R. Belosludov, R.V. Belosludov and Y. Kawazoe, *Nature*, **400**, 647, (1999).

[59] D.D. Klug, C.A. Tulk, E.C. Svensson and C.-L. Loong, *Phys. Rev. Lett.*, **83**, 2584, (1999).

[60] G.P. Johari, *J. Chem. Phys.*, **112**, 8573, (2000).

[61] V.P. Shpakov, P.M. Rodger, J.S. Tse, D.D. Klug, and V.R. Belosludov, *Phys. Rev. Lett.*, **88**, 155502, (2002).

[62] T. Springer, *Quasielastic neutron scattering for the investigation of diffusive motions in solids and liquids*, in "Springer Tracts in modern physics No.64", Springer Verlag, (1972).

[63] M. Bee, *Quasielastic Neutron Scattering*, Adam Hilger, (1988).

[64] S.W. Lovesey, *Theory of Neutron Scattering from Condensed Matter*, Oxford Science Publications, (1984).

[65] B. Geil, M.M. Koza, F. Fujara, H. Schober, and F. Natali, *Phys. Chem. Chem. Phys.*, **6**, 677, (2004).

[66] The Yellow-Book *Guide to neutron research facilities at the ILL*, ILL, 1994.

[67] M.M. Koza, H. Schober, H.E. Fischer, T. Hansen, and F. Fujara, *J. Phys.: Condens. Matter*, **15**, 321, (2003).

[68] M.M. Koza, H. Schober, T. Hansen, A. Tölle and F. Fujara, *Phys. Rev. Lett.*, **84**, 4112, (2000).

[69] J. Wuttke, *Phys. Rev. E*, **62**, 6531, (2000).

[70] Please note that, although coherent and incoherent scattering has been exploited in this work we do not distinguish between the Mössbauer-Lamb and the Debye-Waller factor in the nomenclature. The last is used exclusively throughout the text.

[71] In the energy range accessed in the present experiments the dynamic properties of the samples

are determined by vibrational modes of water molecules ($\hbar\omega < 40$ meV). The number of scatterers N and their mass M can be therefore related to the water molecule.

- [72] N.D. Ashcroft, and N.W. Mermin, *Solid State Physics*, Sounders College Philadelphia, (1976).
- [73] Please note, that the formation of ice I_h cannot be characterised by a specific transition temperature. The step at $T \approx 240$ K in our data results from the thermal treatment, i.e. the heating rate, applied during the measurement. The formation of ice I_h is stretched over a wide range of temperatures and was observed by us in other experiments on longer time scales already at about 200 K.
- [74] W. Hage, A. Hallbrucker, E. Mayer, and G.P. Johari, *J. Chem. Phys.*, **100**, 2743, (1994).
- [75] W. Hage, A. Hallbrucker, E. Mayer, and G.P. Johari, *J. Chem. Phys.*, **103**, 545, (1995).
- [76] A. Ermolieff, *Solid State Comm.*, **17**, 1013, (1975).
- [77] A.J. Leadbetter, *Proc Roy. Soc. A*, **287**, 403, (1965).
- [78] W. Reichardt, *Muphocor, a fortran program to determine the phonon density of states from neutron scattering experiments*, Kernforschungszentrum Karlsruhe GmbH, No.13.03.01p06L, (1984).
- [79] M.M. Bredov, B.A. korov, N.M. Okuneva, V.S. Oskotskii, and A.L. Shakh–Budagov, *Sov. Phys. Solid State*, **9**, 214, (1967).
- [80] V.S. Oskotskii, *Sov. Phys. Solid State*, **9**, 420, (1967).
- [81] S.N. Taraskin, and S.R. Elliot, *Phys. Rev. B*, **55**, 117, (1997).
- [82] M.M. Koza, et al., *Collective dynamics and inelastic properties of ice XII.*, in preparation.
- [83] E.L. Gromnitskaya, O.V. Stal'gorova, V.V. Brazhkin and A.G. Lyapin, *Phys. Rev. B.*, **64**, 94205, (2001).
- [84] R.E. Gagnon, H. Kiefte, M.J. Clouter and E. Whalley, *J. Chem. Phys.*, **92**, 1909, (1990).
- [85] The estimation of the transverse and longitudinal velocity of sound for LDA and I_c from [83] is difficult due to their variation during the heat treatment of the sample and the data collection. Therefore we encourage the readers to estimate the Debye temperature themselves. The values estimated by us are:
HDA: $v_t = 2.04$ km/s, $v_l = 3.73$ km/s,
LDA: $v_t = 1.92$ km/s, $v_l = 3.67$ km/s,
ice I_c : $v_t = 1.92$ km/s, $v_l = 3.77$ km/s.
- [86] D.D. Klug, E. Whalley, E.C. Svensson, J.H. Root, and V.F. Sears, *Phys. Rev. B*, **44**, 841,

(1991).

[87] It is noteworthy, that the TAS experiments exploit the Stokes line, i.e. the neutron energy loss side, whereas TOF experiments performed by our group utilise the anti-Stokes side, i.e. the neutron energy gain side. The difference between the TAS and TOF experiments is manifested by the temperature dependence of the detailed balance factor [64], which results in a lower sensitivity of the TOF experiments to the rather high energy $\hbar\omega \approx 2$ meV of the TLS. In the elastic mode, the back-scattering spectrometers IN13 and IN16 are sensitiv to both, the Stokes and the anti-Stokes line, whereby the incident energy of neutrons determines the maximum energy range on the Stokes side.